



HAL
open science

Investigating the use of fallout and geogenic radionuclides as potential tracing properties to quantify the sources of suspended sediment in a mining catchment in New Caledonia, South Pacific

Virginie Sellier, Oldrich Navratil, J. Patrick Laceby, Michel Allenbach, Irène Lefèvre, O. Evrard

► To cite this version:

Virginie Sellier, Oldrich Navratil, J. Patrick Laceby, Michel Allenbach, Irène Lefèvre, et al.. Investigating the use of fallout and geogenic radionuclides as potential tracing properties to quantify the sources of suspended sediment in a mining catchment in New Caledonia, South Pacific. *Journal of Soils and Sediments*, 2020, 20, pp.1112-1128. 10.1007/s11368-019-02447-8. hal-02399278

HAL Id: hal-02399278

<https://hal.science/hal-02399278>

Submitted on 28 May 2020

HAL is a multi-disciplinary open access archive for the deposit and dissemination of scientific research documents, whether they are published or not. The documents may come from teaching and research institutions in France or abroad, or from public or private research centers.

L'archive ouverte pluridisciplinaire **HAL**, est destinée au dépôt et à la diffusion de documents scientifiques de niveau recherche, publiés ou non, émanant des établissements d'enseignement et de recherche français ou étrangers, des laboratoires publics ou privés.

2 **Investigating the use of fallout and geogenic radionuclides as potential tracing properties to quantify the**
3 **sources of suspended sediment in a mining catchment in New Caledonia, South Pacific**

4

5 **Virginie Sellier¹ • Oldrich Navratil² • J. Patrick Lacey³ • Michel Allenbach⁴ • Irène Lefèvre¹ • Olivier**
6 **Evrard¹**

7

8 ¹Laboratoire des Sciences du Climat et de l'Environnement (LSCE), UMR 8212 (CEA/CNRS/UVSQ-IPSL),
9 Université Paris-Saclay, Gif-sur-Yvette, France

10 ²Laboratoire Environnement-Ville-Société (EVS), UMR 5600/IRG, Université Lumière Lyon 2, Lyon (France)

11 ³Environmental Monitoring and Science Division (EMSD), Alberta Environment and Parks (AEP Calgary,
12 Alberta, Canada

13 ⁴LIVE-EA 4243, Université de Nouvelle-Calédonie, Nouméa, (Nouvelle-Calédonie, France) & LABEX Corail,
14 France

15

16

17 ✉ Virginie Sellier

18 virginie.sellier@lsce.ipsl.fr

19

20 **Abstract**

21 *Purpose.* New Caledonia, a French island located in the south-west Pacific Ocean, has vast nickel resources.
22 Open-cast mining has strongly increased soil erosion and the subsequent downstream transfer of sediments in
23 river systems resulting in fundamental morphological changes (e.g. hyper-sedimentation, over-burden).
24 Understanding the sediment source contributions from mining activities is therefore important to guide the
25 implementation of effective management measures.

26 *Materials and methods.* A pilot sediment tracing study was conducted in the Thio River (400 km²) catchment
27 draining the island's first mine. Sediment deposited during the February 25, 2015 and April 10, 2017 flood
28 events was collected with a tributary tracing design, including main stem (n=19) and tributary (n=24) samples.
29 The tributaries were classified into two source types: sub-catchments draining mining sites and sub-catchments
30 devoid of mining activities. Three sets of potential tracing parameters (i.e. fallout radionuclides, geogenic
31 radionuclides, and elemental geochemistry) were examined for their potential to model the contributions of
32 sediment from mining versus non-mining tributaries to sediment collected on the Thio River.

33 *Results and discussion.* The very low fallout radionuclide activities (¹³⁷Cs and ²¹⁰Pb_{xs}) found in the source and
34 sediment samples demonstrate that most material transiting the river network is derived from subsoil sources.
35 Geogenic radionuclides and elemental geochemistry were therefore utilized in the tributary tracing approach.
36 Accordingly, U and K were selected as the optimal tracers of the two main lithological regions supplying
37 sediment to the main stem of the Thio River. Model results demonstrated that tributaries with mining activity
38 dominated the sediment supply to the Thio River with mean sediment contributions of 68 % (SD 28 %) for the
39 2015 flood and 86 % (SD 7 %) for the 2017 event.

40 *Conclusions and perspectives.* Geogenic radionuclides and elemental geochemistry were more effective at
41 discriminating between tributaries with and without mines than fallout radionuclides. The similarity of the model
42 results from tracing with geogenic radionuclides and elemental geochemistry illustrates their potential to
43 investigate sediment source contributions in similar catchments across the South Pacific Islands affected by
44 mining activities.

45 **Keywords** Caesium-137 • Nickel mining • Sediment source fingerprinting • Soil erosion • X-ray fluorescence

46

47 **1. Introduction**

48 Soil erosion and the associated sediment transfer to river systems are exacerbated in tropical regions
49 exposed to heavy rainfall, particularly during cyclones (Mertes 1994; Aalto and Nittrouer 2012). In the South
50 Pacific region, including the French Island of New Caledonia, these tropical depressions frequently generate
51 overbank peak flows that may damage human settlements, public infrastructure and agricultural land (Terry et al.
52 2008). The flood events generated by cyclones and tropical depressions supply the major part of the sediment
53 flux transiting rivers in this region. For example, during significant rainfall events, riverine suspended sediment
54 concentrations (SSC) have exceeded concentrations of 350 g L^{-1} resulting in high sedimentation rates ($> 3 \text{ cm yr}^{-1}$)
55 on floodplains in Fiji (Terry et al. 2002).

56 In New Caledonia, a significant proportion of the sediment load is potentially generated by mining
57 activities, which increase the terrigenous inputs to downstream coastal lagoons (Bird et al. 1984). Although the
58 mining sector has contributed to the economic growth of New Caledonia since the 1880s (5 % of GDP (IEOM
59 2016)), it is also considered to be the one of the main drivers of environmental degradation on the island
60 (Sabinot and Lacombe 2015).

61 Suspended sediment is known to transport large quantities of nutrients and contaminants in river
62 systems (Owens et al. 2001; Owens and Walling 2002; Walling et al. 2003). In New Caledonia, high
63 concentrations of trace metals, including Ni and Cr, were found in pelagic and freshwater organisms (Hedouin et
64 al. 2007; Hedouin et al. 2008). In addition, the suspended sediment itself degrades coral reef systems (Rogers
65 1990). Coral reefs are particularly sensitive to increases in turbidity as they often become stressed by the
66 reduction in light penetration (Rogers 1979; Heintz et al. 2015; Restrepo et al. 2016). The degradation of 4500
67 km^2 of Caledonian coral reefs, listed as a UNESCO World Heritage site, threatens a variety of fundamental
68 ecosystem services (e.g. fisheries, coastal protection and tourism) estimated at a value of \$340 million USD per
69 year (Pascal 2010).

70 To protect these natural resources, the effective management of mining resources is required (Pascal et al.
71 2008; David et al. 2010). Open-cast mining is widespread in New Caledonia. The island's soils, developed on
72 ultrabasic rocks (e.g. peridotites), are enriched in Fe and transition metals such as Mn, Ni, Cr and Co
73 (Schwertmann and Latham 1986). The weathering of the peridotite results in the formation of Ni- and Fe-rich
74 smectite, serpentine, goethite and hematite. The migration of these transition metals through the soil profile
75 results in higher Ni concentrations in the saprolite (Ni: 0.5-3.5 %) and laterite layers (Ni: 0.9-1.8 %) (Trescases
76 1973). Both saprolite and laterite are mechanically mined, generating large quantities of overburden material

77 (e.g. mining tailings). This mining waste was historically (i.e. since 1880) stored on the foothills of the mines. In
78 1975, the inhabitants of New Caledonia, whose livelihood was already impacted by heavy rainfall events,
79 became increasingly aware of the deleterious consequences of mining activities due to cyclone Alison, which
80 generated extensive flooding and mudflows across the island.

81 Although the management of overburden material was improved through the prohibition of mining waste
82 storage on foothills and the creation of storage ponds on the mining sites after 1975, a significant quantity of
83 legacy material has accumulated on the hillsides where it is frequently exposed to erosion processes. In addition
84 to these mining-related inputs of both fine sediment and coarser materials, other sources of sediment may supply
85 a significant quantity of particulate material to New Caledonian river systems. Bushfires or land-clearing fires
86 occur frequently in the region (Dumas et al. 2010). These fires can lead to shallow landslides and/or extensive
87 soil erosion of surface material on hillslopes (Blake et al. 2009; Nyman et al. 2011; Smith et al. 2012).
88 Moreover, the deer population significantly increased during the last 40 years. The associated trampling may
89 have further accelerated surface soil degradation (Shellberg et al. 2010).

90 To help improve the management of deleterious sediment loads in mining-affected regions in New
91 Caledonia, it is important to improve our understanding of the main sediment sources. Sediment fingerprinting
92 techniques have been widely applied to investigate the relative contribution of multiple sources (Walling et al.
93 1979; Collins et al. 1996; Walling 2005). These techniques can provide information on the main erosion
94 processes involved in sediment mobilization (e.g. mass movement, sheet, rill, gully and channel erosion) and the
95 spatial origin of sources (e.g. land-use, lithology) that cannot be provided by traditional monitoring techniques.
96 They consist of the measurement of multiple conservative properties, or fingerprints, in both sediment sources
97 and river sediment in order to quantify the respective source contributions to material transiting river systems
98 (Davis and Fox 2009; Koiter et al. 2013; Walling 2013). The commonly used properties can be grouped into four
99 main categories; geochemical (e.g. elemental geochemical contents, isotopic ratios), biogeochemical (e.g.
100 organic compounds), physical (e.g. mineral, magnetic parameters) and nuclear properties (e.g. radioactive
101 elements) (Koiter et al. 2013). In recent years, these latter have diversified with the emergence of more
102 alternative sediment fingerprinting techniques based on sediment color (Martínez-Carreras et al. 2010; Legout et
103 al. 2013), pollen plant (Brown et al. 2008) or more recently environmental DNA (Ficetola et al. 2018; Evrard et
104 al. 2019). This diversity in the use of fingerprints has been achieved in conjunction with the improvement of
105 mixing models (e.g. reduction of associated uncertainties). Following this progress, Laceby et al. (2019)
106 recommend to further develop the combination of multiple sets of fingerprints to enrich the knowledge base of

107 these parameters and the associated potential biases (e.g. source variability, particle size selectivity). These
108 authors outlined in particular the need to improve our understanding of processes that establish the source
109 fingerprint signals and their conservative behavior in order to be able to provide a better analysis of key
110 processes driving the mobilization, generation, and deposition of sediment.

111 In New Caledonia, sediment originates from two main sources. In areas affected by bushfires and
112 grassland degradation, sediment may be derived from a mixture of surface material (e.g. hillslope erosion) and
113 subsurface soils (e.g. shallow landslides and channel bank erosion). In contrast, sediment associated with mining
114 activities (e.g. overburden, bare mining soils, mining prospection and access roads) will likely consist
115 predominantly of subsurface material. One potential approach to discriminate between surface and subsurface
116 sediment sources is the comparison of their fallout radionuclide activities (^{137}Cs , $^{210}\text{Pb}_{\text{xs}}$). In particular, ^{137}Cs
117 ($t_{1/2} = 30$ years), a by-product of thermonuclear bomb testing, which mainly occurred between 1952–1974 in the
118 Southern Hemisphere, was demonstrated to be an effective tracer of surface and subsurface sources in numerous
119 studies conducted in nearby Australia (Olley et al. 2013; Wilkinson et al. 2013; Hancock et al. 2014).
120 Accordingly, ^{137}Cs could potentially discriminate between mining and non-mining sources, the latter of which is
121 hypothesized to have higher ^{137}Cs concentrations owing to a greater proportion of surface material.

122 In addition to the investigation of fallout radionuclide analyses, the inclusion of other tracers including
123 geochemical elements (Koiter et al. 2013; Laceby et al. 2015; Batista et al. 2018) holds potential to provide
124 additional sediment source information such as whether non-mining or mining sources dominate the supply of
125 sediment. Peridotite massifs where nickel ores are extracted cover one third of the island and are characterized
126 by a depletion of Th, K and U. Contrarily, the volcano-sedimentary formation, that covers approximately the
127 remaining two thirds of the island, are naturally enriched in Th, K and U (Sevin 2014). Accordingly, the Th, K
128 and U contents may discriminate between sediment contributions from tributaries draining mines compared to
129 watercourses flowing across areas devoid of mining activities.

130 The objective of this research is to quantify the contribution of mining and non-mining tributaries to the
131 Thio River, one of the first catchments in New Caledonia to be mined for nickel. In particular, three sets of
132 potentially discriminant tracing properties will be tested to quantify sediment source contributions: fallout
133 radionuclides (i.e. ^{137}Cs and $^{210}\text{Pb}_{\text{xs}}$), geogenic radionuclides (i.e. Th, K and U) and elemental geochemistry. The
134 model results will quantify the relative contribution of mining tributaries to sediment loads degrading the Thio
135 River and its estuary. The results will also help to develop an approach to examine source contributions from

136 mining/non-mining catchments across New Caledonia and potentially across similar South Pacific and other
137 tropical islands.

138

139 **2. Materials and methods**

140 *2.1. Study area*

141 The New Caledonian archipelago is located in the southwestern Pacific Ocean, in Melanesia. The Thio
142 River catchment (397 km²) is located on the east coast of the main island, called La Grande-Terre (17,000 km²).
143 The catchment has a variable topography, with a mean altitude of 416 m asl (above sea level); ranging from 0 to
144 1352 m asl (Figure 1-b). On the western part of the catchment, volcanoclastic sandstone, clay rock and magmatic
145 rock formations are composed of cherts (22 %), sandstone (9 %), a mix of basalt, dolerite and gabbro (6 %),
146 polymetamorphic rocks (6 %) and alluvia (4 %). Laterites (18 %), peridotites (17 %), serpentines (10 %) and
147 hazburgites (1 %) constitute the peridotite massifs, which mainly cover the eastern part of the catchment (40 %
148 of the catchment surface), which results in its steeper relief (Garcin et al. 2017) (Figure 1-a). The main land use
149 in the catchment is permanent vegetation including forests (37 %), shrubland (35 %) and bushland (18 %) (Alric
150 2009). According to the mining registry, mining concessions cover 40% of the catchment area including 21%
151 (Figure 1-c) corresponding to active and abandoned mining sites and exploration.

152 The climate is tropical and is characterized by the alternation of a hot wet season (November-April;
153 mean temperature of 27 °C) and a cooler dry season (May-October; mean temperature of 20 °C). The mean
154 annual rainfall in the Thio catchment is 1620 mm (1981–2008) (Alric 2009). About fifty cyclones have affected
155 New Caledonia since the 1880s (i.e. a cyclone or a tropical depression occurs on average every 2.7 years)
156 (Garcin 2010). According to local meteorological records, cyclones may supply more than 20 % of the annual
157 rainfall in only one day (Météo France).

158 The catchment's river network is dense with 12 tributaries (Figure 1-b) flowing into the main stem of
159 the Thio River (28 km long). Ninety-two percent of the river channel length is characterized with a slope lower
160 than 5 %. The overall slope index I_g (34 ‰) reflects the torrential regime observed in the Thio River tributaries.
161 The catchment is very reactive to heavy rainfall given the extensive bare soil surface associated with past mining
162 activities (~10 sites), ongoing mining operations (e.g. 2 sites: *Thio Plateau*, *Camp des Sapins*) and the
163 occurrence of 6 km² of mining roads, which all increase runoff production as they are well connected to the river
164 network (Alric 2009). Extensive erosion processes are evident across the Thio catchment, including rills, gullies,
165 landslides and channel bank erosion (Danloux and Laganier 1991).

166

167 2.2. Hydro-sedimentary monitoring

168 Rainfall is recorded at three stations (i.e. Thio Plateau, Thio village, Camps des Sapins) operated by
169 Météo France and five stations by the island's local authorities (i.e. Kouaré, Bel-Air, Ningua, Kuenthio, Mont
170 Do managed by the DAVAR – Direction des Affaires Vétérinaires Alimentaires et Rurales), with records
171 available since 1952. Rainfall data at these eight stations was collected for two floods investigated in the current
172 research, the tropical depression on February 25, 2015 and Cyclone Cook on April 10, 2017. Daily discharge has
173 been monitored at a river gauging station located on the main stem of the Thio River section (at Saint-Michel)
174 since 1981 by the DAVAR (Figure 1-b).

175

176 2.3. Source and river sediment sampling

177 A tributary tracing design was used to investigate sediment source contributions in the Thio River
178 catchment (Olley and Caitcheon 2000; Evrard et al. 2015; Laceby et al. 2017). The tributary approach consists of
179 sampling sediment in the different tributaries and using these samples as potential sources of sediment sampled
180 further downstream on the main stem of the Thio River (Figure 1-c). Using lag deposits as potential source
181 samples is a common technique in sediment fingerprinting studies (Bottrill et al. 1999). For those catchments
182 that are not equipped with automatic sediment such as the Thio River catchment, lag deposit sampling is the
183 most suitable alternative for suspended sediment sampling, particularly because it is well representative of the
184 whole catchment area. Olley et al. (2013) showed that equivalent results (i.e fallout radionuclide activities) were
185 observed for both lag deposits and suspended sediment samples (i.e. <10 µm fraction). However, this sampling
186 technique also has disadvantages such as those outlined by Haddadchi et al. (2013), and including a lack of
187 information on the hysteresis effect of flood events and the effect of discharge on sediment contribution from
188 different sources.

189

190 Lag deposits were collected at exposed subaerial sites free of vegetation on channel bars. Forty-three
191 samples were collected after two major floods (~10 yr return period): (1) the tropical depression of February 25,
192 2015 with lag deposits sampled between April 30 and May 5, 2015 ($n=31$) and (2) Cyclone Cook on April 10,
193 2017, sampled between May 16 and 17, 2017 ($n=12$). At each sampling site, five to ten subsamples of fine
194 sediment were collected across a 10-m² surface with a plastic trowel. The subsamples were composited into one
195 sample representative of the fine sediment deposited on the channel bars. Among these samples, 16 were

196 collected in tributaries with mine activities ('mining tributaries'), eight in tributaries draining areas devoid of
197 mining activities ('non-mining tributaries') and 19 on the main stem of the Thio River (Figure 1-c). The samples
198 were oven-dried at 40°C for ~48 hours and sieved to 2 mm and 63 µm.

199

200 2.4. Source and river sediment analysis

201 2.4.1. Particle size

202 Fine particles are preferentially mobilized and transported over longer distances. This process may lead
203 to the accumulation of finer particles in the lower reaches of the main river channel and receiving waters. In the
204 Thio catchment, this phenomenon has resulted in the hyper-sedimentation observed in the main stem and the
205 lagoon. This particle size selectivity may affect biogeochemical properties (i.e. geochemical transformations,
206 organic matter depletion/enrichment) and physical properties (i.e. particle size) of source and downstream
207 sediment material (Lacey et al. 2017). Different techniques were implemented to address particle size effects in
208 sediment fingerprinting studies (e.g. fractionation of source and sediment material to a narrow particle size
209 range, concentration corrections) (Stout et al. 2013; Foucher et al. 2015; Le Gall et al. 2016). In the current
210 research, fallout radionuclide activities, geogenic radionuclide and geochemical element contents measured in
211 the <2 mm and <63 µm fractions of samples were compared. Gamma spectrometry and X-ray fluorescence
212 analyses were carried out on a subset of samples (n=31) for which both fractions were analyzed. Linear
213 correlations between the parameters measured in <2 mm and <63 µm fractions was assessed to select properties
214 that were the less affected by a potential particle size effect.

215

216 2.4.2. Gamma spectrometry

217 Tributary and main stem samples (n=43) were packed in 15 mL polyethylene containers for
218 radionuclide analysis with gamma spectrometry using coaxial N- and P-type HPGe detectors (Canberra/Ortec) at
219 the Laboratoire des Sciences du Climat et de l'Environnement (LSCE, Gif-sur-Yvette, France). ¹³⁷Cs activities
220 were measured at the 662 keV emission peak. ²¹⁰Pb_{xs} activities were calculated by subtracting the supported
221 activity (determined by using two ²²⁶Ra daughters), ²¹⁴Pb (average count number at 295.2 and 351.9 keV) and
222 ²¹⁴Bi (609.3 keV)) from the total ²¹⁰Pb activity measured at 46.5 keV (Le Gall et al. 2017). Assuming that ²³²Th
223 and its daughter products were in secular equilibrium, ²²⁸Th activities were calculated using the average between
224 the gamma rays of two of its daughter products, ²¹²Pb (239 keV) and ²⁰⁸Tl (583 keV) (Le Gall et al. 2016).
225 Elemental concentrations in Th (mg kg⁻¹) were calculated from ²²⁸Th activities. In the same way, ²³⁸U was

226 estimated from the gamma rays of its daughter, ^{214}Pb (295 and 352 keV) and the U elemental content was
227 expressed in mg kg^{-1} . ^{40}K was detected at 1460 keV and the K concentration was provided in mg kg^{-1} . Counting
228 efficiencies and calibration were conducted using certified International Atomic Energy Agency (IAEA)
229 standards (IAEA-444, 135, 375, RGU-1 and RGTh-1) prepared in the same containers as the samples.

230

231 2.4.3. *X-ray fluorescence*

232 X-ray fluorescence measurements were conducted on sediment samples stored in air double X-ray Mylar
233 film small mass holder cells with a sample quantity between 0.2 and 0.5g. Major element contents (i.e. Mg, Al,
234 Si, K, Ca, Ti, Cr, Mn, Fe, Ni, Cu, Co and Zn) were analyzed by energy dispersive X-ray fluorescence
235 spectrometry (Epsilon 3, Malvern PANalytical) at LSCE, Gif-sur-Yvette, France. Samples were irradiated by a
236 primary beam generated by an Rh anode X-ray tube emitting electromagnetic waves between 100eV and 1MeV
237 with a maximum power, typical current and voltage fixed to 15 W, 3mA and 50 kV respectively. The associated
238 Si-drift detector had a Be window thickness of 8 μm and recorded the sample spectrum in a 2D optical geometry
239 configuration. Between 8 and 16 certified reference samples including Internal Atomic Energy Agency (IAEA)
240 standards were used to derive the calibration curves for the geochemical elements of interest. X-ray intensities
241 were converted into concentrations using the Epsilon 3 software program through the application of the
242 fundamental parameters method. Correlations between the determined and the standard elemental contents were
243 comprised between 0.90 And 0.99. To validate the calibration, three certified samples different from those used
244 for the calibration were analysed, and the associated mean relative error was 17 % (SD 5 %). Due to imprecise
245 calibration for Co (error: 264 %), this element was removed from further analysis.

246

247 2.5. Conservative behavior and source discrimination

248 A multi-parameter composite fingerprinting approach was developed by Collins et al. (1996) to identify
249 the spatial sediment sources and quantify their contributions in the river network. This approach first selects an
250 optimal suite of tracers that discriminate different sediment sources. Second, this approach estimates the relative
251 source contributions to target sediments using end member mixing models.

252 The fingerprinting technique relies on the ability of tracers to discriminate between sediment sources
253 while remaining conservative. The use of non-conservative tracers may lead to incorrect source group prediction
254 resulting in inaccurate estimations of source contributions (Sherriff et al. 2015). Accordingly, it is generally
255 considered important to restrict the tracing parameters to those that demonstrate conservative behavior.

256 Therefore, each set of potential tracing properties (i.e. fallout radionuclides, geogenic radionuclides and
257 elemental geochemistry) was plotted to ensure that the tributary source properties plotted within the source
258 range.

259 Thereafter, the Mann-Whitney U-test ($\alpha=0.05$) selected parameters that significantly discriminated
260 between the two sediment sources (i.e. mining and non-mining tributaries) for each group of potential tracers. A
261 stepwise discriminant function analysis (DFA; $\alpha=0.05$) was then used to select the optimal number of potential
262 tracers through the selection of those that collectively maximized the discrimination between both sediment
263 sources for each set of tracers. The optimal tracers for modelling were selected by minimizing the Wilks' lambda
264 values in the backwards mode, with a $p<0.05$ used to select a tracer and $p<0.10$ used to remove a tracer.

265

266 2.6. Source contribution modelling

267 A distribution modelling approach was used to model the source contributions from the mining and non-
268 mining tributaries to target sediment (Lacey et al. 2015; Lacey and Olley 2015). This approach incorporates
269 distributions throughout the entire modelling framework, including the source contribution terms and the target
270 sediment. For this two-source model, it is assumed that sediment samples constitute a discrete mixture of their
271 sources, with the contribution from Source A being x , and the contribution of Source B being $(1-x)$ where:

$$272 Ax + B(1 - x) = C \quad \text{Equation 1}$$

273 C is the target Thio river sediment distribution, A and B are again the two source distributions (i.e. mining and
274 non-mining tributaries), and x is modelled as a truncated normal distribution ($0 \leq x \leq 1$) with a mixture mean
275 (μ_m) and standard deviation (σ_m) (Lacey and Olley 2015). The model is solved by minimizing the median
276 difference between the distributions of both sides of Equation 1 (e.g. C and $Ax + B(1 - x)$) with the Optquest
277 algorithm in Oracle's Crystal Ball software with a randomly generated mixture mean (μ_m) and standard
278 deviation (σ_m). Source contributions (x) were determined by simulating all distributions in Equation 1 with
279 2500 Latin Hypercube samples from 500 bins and varying the mixture mean (μ_m) and standard deviation (σ_m).
280 This simulation and solving procedure repeated 2500 times and the median proportional source contribution
281 from these 2500 additional simulations being reported as the source contribution to the target sediment.
282 Uncertainty was determined through summing three quantifiable model uncertainties: (1) the median absolute
283 deviation of the individual source median contribution for the additional 2500 simulations; (2) the modelled
284 standard deviation; and (3) the median absolute deviation of this modelled standard deviation for the 2500 model
285 additional simulations (Lacey et al. 2015).

286

287 3. Results

288 3.1. Conservative behavior and source discrimination

289 3.1.1 Fallout radionuclides

290 Although the samples were analyzed in an ultra-low background laboratory, fallout radionuclide activities
291 (i.e. ^{137}Cs , $^{210}\text{Pb}_{\text{xs}}$) were below detection limits for 10 samples for ^{137}Cs , and 5 samples for $^{210}\text{Pb}_{\text{xs}}$ for <2 mm
292 fraction of samples (Table 1). When analyzing the <63 μm fraction, the results remained below detection limits
293 for five sediment samples for ^{137}Cs and for two samples for $^{210}\text{Pb}_{\text{xs}}$. For the samples above the detection limit,
294 mean activities for ^{137}Cs were 0.3 Bq kg^{-1} (SD 0.3 Bq kg^{-1}) for mining sources. Slightly higher mean ^{137}Cs
295 activities were measured in non-mining sources (1 Bq kg^{-1} ; SD 0.5 Bq kg^{-1}). Similar values were found in the
296 Thio River target sediment samples (i.e. on the main stem) in 2015 (0.7 Bq kg^{-1} ; SD 0.4 Bq kg^{-1}) (Table 1, <63
297 μm fraction). $^{210}\text{Pb}_{\text{xs}}$ activities were lower in mining sources (6 Bq kg^{-1} ; SD 7 Bq kg^{-1}) compared to non-mining
298 sources (19 Bq kg^{-1} ; SD 15 Bq kg^{-1}). $^{210}\text{Pb}_{\text{xs}}$ activities in the Thio River target sediment samples were similar to
299 non-mining sources in 2015 (15 Bq kg^{-1} ; SD 8 Bq kg^{-1}) (Figure 2-b, Table 1, <63 μm fraction).

300 Fallout radionuclide activities measured in both <63 μm and <2 mm fractions of sediment were
301 correlated; with r^2 coefficients of 0.66 for ^{137}Cs and 0.73 for $^{210}\text{Pb}_{\text{xs}}$ (Figure 3-a, b). Owing to particle size effect
302 affecting fallout radionuclides activities (Figures 2 and 3, Table 1) and a larger number of results above the
303 detection limits in the <63 μm fraction, the sediment fingerprinting approach was carried out exclusively on the
304 finest fraction of samples. ^{137}Cs and $^{210}\text{Pb}_{\text{xs}}$ activities found in river sediment samples plotted within the range of
305 activities measured in the potential source samples, indicative of conservative behavior (Figure 2-b). However,
306 the p-values associated with the Mann-Whitney U test ($\alpha=0.05$, $p<0.1$) for both ^{137}Cs (0.7720) and $^{210}\text{Pb}_{\text{xs}}$
307 (0.1109) indicated that these tracers were not able to significantly discriminate between sediment sources (i.e.
308 mining and no-mining tributaries). Accordingly, fallout radionuclides were not used to model sediment source
309 contributions in the Thio River catchment.

310

311 3.1.2 Geogenic radionuclides

312 There were 10-fold higher Th, U, K contents found in non-mining source samples compared to mining
313 source samples (Figure 4, Table 1, <2 mm). Mean Th contents were 6 mg kg^{-1} (SD 2 mg kg^{-1}) in non-mining
314 source samples versus 0.6 mg kg^{-1} (SD 0.7 mg kg^{-1}) for mining source samples. Mean K content was $12,097 \text{ mg}$
315 kg^{-1} (SD 3980 mg kg^{-1}) for non-mining source samples relative to 1386 mg kg^{-1} (SD 1848 mg kg^{-1}) in mining

316 source samples. Finally, mean U contents were 1.2 mg kg⁻¹ (SD 0.3 mg kg⁻¹) in non-mining sources and 0.1 mg
317 kg⁻¹ (SD 0.1 mg kg⁻¹) in mining source samples (Table 1). Target river sediment samples were characterized by
318 low geogenic radionuclide contents, similar to those found in mining source samples (Figure 4). These contents
319 remained similar in sediment collected after both 2015 and 2017 flood events (Figure 4, Table 1). Mean Th
320 contents in the Thio River sediment samples were 1 mg kg⁻¹ (SD 0.6 mg kg⁻¹) in 2015 and 2 mg kg⁻¹ (SD 1 mg
321 kg⁻¹) in 2017. Mean K content was 4711 mg kg⁻¹ (SD 2270 mg kg⁻¹) in 2015 relative to 2792 mg kg⁻¹ (SD 880 mg
322 kg⁻¹) in 2017. Finally, mean U contents were 0.3 mg kg⁻¹ (SD 0.1 mg kg⁻¹) in 2015 and 0.4 mg kg⁻¹ (SD 0.3 mg
323 kg⁻¹) in 2017 (Table 1, <2 mm).

324 Analyses conducted on the <2 mm and <63 µm fractions (n = 31) demonstrated that Th, K and U
325 contents were very well correlated in fine and coarse material (r²=0.96, 0.92, 0.90 respectively) (Figure 5-a, b, c).
326 Accordingly, these geogenic radionuclide properties were considered not to be significantly impacted by a
327 potential particle size effect. As the elements were highly correlated between the two particle size fractions, the
328 <2 mm was used in the modelling process.

329 According the Mann-Whitney U test results, all three geogenic radionuclides provided significant
330 discrimination between the sediment sources (i.e. p-value < 0.1, Table 2). U was selected by the DFA to model
331 sediment source contributions from mining and non-mining tributaries (Table 2) with a Wilk's lambda value was
332 0.1742 and 96 % of sources correctly classified.

333

334 3.1.3 Geochemistry

335 The concentrations of several geochemical elements were higher in mining source samples compared to
336 non-mining sources, with 17-fold higher levels of Ni, 10-fold higher levels of Cr, 5-fold higher levels of Mg and
337 two-fold higher concentrations of Fe and Mn (Figure 6). On the contrary, K, Ti and Al were enriched in non-
338 mining source samples compared to mining sources, with 8-fold higher K concentrations, 3-fold higher Ti
339 concentrations and two-fold Al concentrations. Zn contents were similar in both source types, with mean
340 concentrations of 125 mg kg⁻¹ (SD 4 mg kg⁻¹) in non-mining sources compared to 146 mg kg⁻¹ (SD 47 mg kg⁻¹)
341 in mining sources. Elemental concentrations measured in the river sediment samples generally plotted closer to
342 the levels measured in mining sources compared to non-mining sources (Figure 6). They were similar in deposits
343 collected in 2015 and 2017, except for the Mg contents that increased (32 %) and the Al and Ti contents that
344 decreased (31 % and 44 %) between both flood events.

345 When comparing measurements on the <2 mm and <63 µm fractions, concentrations in most elements
346 (i.e. Al, Ca, Cr, Fe, K, Mg, Mn, Ni, Si Ti and Zn) were not impacted by particle size (r^2 between 0.77 and 0.99)
347 (Figure 7-a, b, c, e, f, g, h, i, j, k, l). In contrast, Cu contents were not well correlated in both fractions ($r^2=0.35$)
348 (Figure 7-d). Accordingly, Cu was not included in as a potential tracer. As the elements were highly correlated
349 between the two particle size fractions, the <2 mm was used in the modelling process.

350 All ten geochemical elements (i.e. Al, Ca, Cr, Fe, K, Mg, Mn, Ni, Si and Ti) that showed similar
351 concentrations and correlations between the <2 mm and <63 µm fractions significantly discriminated between
352 the potential sediment sources (i.e. Mann-Whitney U test ($\alpha=0.05$, $p<0.1$) (Table 2). The DFA selected K as the
353 optimal tracer of mining and non-mining source sediments with a Wilk's lambda of 0.1691 and 96 % of the
354 source samples were correctly classified (Table 2).

355

356 3.2. Modelling results

357 The geogenic model (U) estimated that 68 % (SD 31 %) of sediment transiting the Thio River during the
358 2015 flood event originated from mining tributaries. Nevertheless, the large standard deviation (31 %) (Table 3)
359 reflects the change of dominant source after different confluence depending on the tributary characteristics. In
360 uppermost areas of the catchment, the contribution of mining tributaries clearly dominated (97 %) (Figure 8,
361 Table 3, [1]). After the confluence with the Kouaré River (Figure 8, [c]), the non-mining sources became the
362 highest (95 %) (Table 3, [3]). Further downstream, the proportions of the mining sources increased again to
363 reach 79 % (Thio Plateau input, Figure 8,[j, k, l], Table 3, [8]). Near the estuary, these mining sources remained
364 largely dominant with sediment contributions between 80-86 % (Table 3, [9-11]).

365 During the 2017 flood event, the geogenic model also estimated that the mining tributaries dominated the
366 supply of sediment throughout the main stem of the Thio River with a mean contribution of 87 % (SD 8 %) (Table 4).
367 The only exception was the Kouaré River which likely supplied a significant contribution of non-
368 mining sediment to the main stem of the Thio River (Figure 9, [c], Table 4, [4]). However, the mining tributary
369 contribution remained dominant in the estuary with a contribution of 86 % (SD 0.1 %) (Figure 9, Table 4, [7-8]).

370 The elemental geochemistry model (K) demonstrated that mining tributaries supplied 68 % (SD 25 %) of
371 the sediment material transiting the Thio River during the 2015 flood event. The results were similar with those
372 obtained with the geogenic model (U): sediment material was mainly supplied by mining tributaries except after
373 the confluence with the Kouaré River where the non-mining sources dominated with a mean contribution of 80
374 % (Table 3, [3]). In the estuary, the mining tributary contribution was estimated to vary between 63-89 % (Table

375 3, [9-11]). The largest difference between both model outputs was 29 % for the 2015 flood (Table 3, [5]). For the
376 2017 flood, results obtained with this model indicated that 84 % (SD 7 %) of sediment material originated from
377 mining tributaries. Along the main stem of the Thio River, mining tributary contributions dominated the supply
378 of sediment (Table 4 [1-8]). Again, the largest difference observed between the results of both models remained
379 low (7 %).

380

381 4. Discussion

382 4.1. Implications for tracing the impact of mining activities on sediment supply in the South Pacific

383 One original assumption of the current research was that fallout radionuclides should provide discrimination
384 between non-mining tributaries, with more surface soil erosion from shallow landslides and areas affected by
385 bushfires and grassland degradation, compared to mining tributaries with higher subsoil erosion from mining
386 related activities including the overburden, bare mining soils and access roads. Accordingly, higher ^{137}Cs and
387 $^{210}\text{Pb}_{\text{xs}}$ activities were expected in potential source samples collected in non-mining tributaries whereas they were
388 assumed to be depleted in mining tributaries where topsoil has been removed to provide access to the laterite and
389 saprolite layers enriched in nickel. However, the results demonstrated low ^{137}Cs and $^{210}\text{Pb}_{\text{xs}}$ activities in both
390 source tributaries. The fallout radionuclide activities in the non-mining tributary sediment were ~10 times lower
391 than those measured in surface sources collected in nearby Australia. Wallbrink et al. (1998) showed that ^{137}Cs
392 and $^{210}\text{Pb}_{\text{xs}}$ activities were comprised between 0.6-3 Bq kg⁻¹ for subsurface sources and 18-270 Bq kg⁻¹ for
393 surface sources when analysing the <2 mm fraction. More recent studies focused on those fallout radionuclide
394 activities contained in the finest fractions (i.e. <63µm and <10µm) of source samples, to which fallout
395 radionuclides are preferentially bound (Smith et al. 2011; Olley et al. 2013; Wilkinson et al. 2013). In these
396 studies, ^{137}Cs and $^{210}\text{Pb}_{\text{xs}}$ activities ranged from 4 to 10 Bq kg⁻¹ for subsurface sources and from 22 to 200 Bq kg⁻¹
397 for surface sources when analysing the <63 µm fraction (Smith et al. 2011). When restricting the analysis to the
398 <10 µm fraction, fallout radionuclide activities were similar to those measured on the <2 mm and <63 µm
399 fractions, varying between 0.15-15 Bq kg⁻¹ for subsurface sources and 10- 150 Bq kg⁻¹ for surface sources (Olley
400 et al. 2013; Wilkinson et al. 2013). Consequently, the low ^{137}Cs and $^{210}\text{Pb}_{\text{xs}}$ activities found in both source
401 tributaries in the current research should likely not to be attributed to the particle size fractions analyzed (<2 mm
402 and <63 µm). On the contrary, Krause et al. (2003) showed that ^{137}Cs activity signatures equivalent to those
403 measured in the Thio River catchment area were rather representative of gullied catchments. The results obtained
404 in the current research indicate that both the mining and non-mining tributaries, and the target sediment collected

405 on the main stem of the Thio River, are derived primarily from subsurface sources. These results are consistent
406 with earlier observations made by Danloux and Laganier (1991) who observed the dominance of subsoil erosion
407 processes in the New Caledonian mining catchments with the widespread occurrence of rills, gullies, landslides
408 and channel bank erosion. These authors also outlined the specific impacts of mining activities conducted during
409 the last 150 years in New Caledonia (e.g. soil stripping over several meters) as responsible for the expansion of
410 these subsoil erosion processes, resulting in the massive supply of sediment to river systems during extreme
411 rainfall events occurring during the cyclone season (i.e. between January and April) (Terry et al. 2002; Terry et
412 al. 2008).

413

414 Despite the occurrence of particle size effects during erosion and sediment transfer processes, the current
415 research showed that a large number of tracers were not impacted by particle size. Geogenic radionuclides (i.e.
416 Th, K, U) and elemental geochemistry (i.e. Al, Ca, Cr, Fe, K, Mg, Mn, Ni, Si, Ti, and Zn) were well correlated in
417 both particle size fractions (i.e. < 2 mm and <63 μm). The geogenic radionuclides are particularly promising as
418 they provide a strong discrimination between both potential sediment sources with very minimal particle size
419 differences. Furthermore, the source discrimination for the geogenic radionuclides is based on a well-established
420 physico-chemical basis. Sevin (2014) reported that, in New Caledonia, the volcano-sedimentary rock formations
421 naturally contained high U and K elemental contents, whereas peridotite massifs were depleted in these
422 elements. As mining sites are concentrated in peridotite massifs, the application of these tracers for identifying
423 the mining source contribution is straightforward. Although U and K trace the lithological regions supplying
424 sediment to the rivers (contributions of peridotite massifs vs. volcano-sedimentary formations), they may also
425 provide indirect information on the land-use contributions. About half of the peridotite massif surface area is
426 occupied by mining exploration, active and abandoned mining sites, whereas these activities are virtually absent
427 from the areas underlain by volcano-sedimentary formations.

428

429 4.2. Spatial and temporal variations of sediment source contributions

430 The geogenic and elemental geochemistry models were based on different fingerprints (i.e. U and K
431 respectively) and particle size fraction analyzes (i.e. <2 mm and <63 μm fractions). Nevertheless, both
432 fingerprinting techniques provided similar estimations of source contributions to sediment even though local
433 differences in modelling results were as high as 29 % (Tables 3 and 4).

434 Although the two investigated events corresponded to floods with a return period of 10 years ($3500 \text{ m}^3\text{s}^{-1}$),
435 they were generated by storms that contributed very different proportions of the annual rainfall (7 % in 2015 vs.
436 25 % in 2017). Furthermore, the spatial pattern of rainfall across the catchment strongly differed. The first event
437 (February 25, 2015) generated more rainfall on the western part of the catchment (230 mm at Kouaré rainfall
438 station vs. 136 mm at Bel-Air rainfall station) (Figure A1-a). The Kouaré River sub-catchment received twice
439 more rainfall than observed in the rest of the Thio River catchment. This heterogeneous spatial rainfall
440 distribution may explain the relatively high contribution of the non-mining source to the sediment deposited in
441 the Thio River after the confluence with the Kouaré River (Figure 8, [c] 80-95 %). On the contrary, rainfall
442 preferentially affected the eastern part of the catchment (409 mm at Thio Plateau station, 493 mm at Camps des
443 Sapins station vs. 60 mm at Kouaré station) during the second event (April 10, 2017) (Figure A1-b). The
444 maximum rainfall was recorded at stations located nearby the mines currently in operation (*Thio Plateau mine*,
445 *Camps des Sapins*) during the cyclone. During this event, the contribution of mining tributaries was larger than
446 that of non-mining tributaries, reducing their relative contribution to 24-27 % (Figure 9, [c]). Although the
447 mining source contributions largely dominated the sediment production across the entire catchment during the
448 two investigated events, the results of the current research showed that the spatial distribution of rainfall may
449 locally or sporadically modify the sediment supply to the river. Nevertheless, the dominant sediment source
450 remained the mining tributaries with contributions varying between 63-82 % during the 2015 event and 84-86 %
451 during the 2017 event near the estuary. These results demonstrate that nickel mining activities directly impact
452 sediment dynamics in this New Caledonia catchment.

453

454 5. Conclusions

455 In New Caledonia, mining activities have been postulated to exacerbate soil erosion and increase
456 sediment transfer to the rivers and the lagoons. In this current study, it was demonstrated that tributaries draining
457 mining sources (e.g overburden, bare mining soils, mining prospection and access roads) dominated the
458 sediment supply to the main stem of the Thio River. During the 2015 event, 68 % (SD 28 %, combined results of
459 both models) of sediment transiting the Thio River originated from mining tributaries. In the 2017 event, the
460 mining tributaries provided 86 % (SD 7 %, combined results of both models) of the sediment input into the main
461 stem of the Thio River. Although the spatial distribution of rainfall was shown to locally modify the respective
462 contributions of non-mining and mining tributaries, the latter provided the main contribution to the sediment
463 collected in the Thio River estuary after both 2015 and 2017 flood events (63-89 %). These results suggest that

464 catchment management should focus on mining tributaries, including those draining the Thio Plateau mine
465 located near the estuary.

466 In this study, substantial efforts were made to address the potential effects of changes in particle size
467 composition (i.e. <63 μm and <2 mm) on sediment properties in a mining catchment. Indeed, detachment,
468 mobilization, transportation and deposition processes did generate a particle size effect illustrated by the
469 differences in fallout radionuclide activities observed in the <63 μm and <2 mm fractions. These results
470 remained consistent with those found in other studies compiled by Laceby et al. (2017). This study also provided
471 additional information on the behaviour of geochemical tracers (i.e. geochemical properties and geogenic
472 radionuclides) in a mining environment, in which very few sediment tracing studies have been conducted so far.
473 Interestingly, geochemical properties and geogenic radionuclide contents were not or only slightly affected by
474 the particle size effect. It would be useful to investigate whether such a conservative behaviour is observed in
475 other mining catchments.

476 Future applications of the sediment tracing technique in mining catchments of New Caledonia and the
477 South Pacific should rely on the measurement of geogenic radionuclide contents and geochemical properties in
478 potential source and sediment material. Furthermore, the current research demonstrated that geogenic
479 radionuclides had the highest discrimination potential between both potential sediment sources. In contrast, the
480 very low fallout radionuclide levels found in sediment analyzed during the current research prevented their use
481 for sediment tracing, although these results illustrated that subsoil erosion dominated in this mining catchment.
482 In the future, additional tracers should be used (e.g. colour, organic matter properties) to provide more detailed
483 source information, in relation with the diversity of land uses and soil types found in similar catchments of the
484 South Pacific Islands in general, and New Caledonia in particular.

485

486 **Acknowledgements**

487 This work was supported by the National Technical Research Center (CNRT) « Nickel and its environment »,
488 Noumea, New Caledonia » (n°10PS2013-CNRT.UNC/IMMILA). Virginie Sellier received a PhD fellowship
489 from the French Atomic Energy Commission (CEA, Commissariat à l’Energie Atomique et aux Energies
490 Alternatives).

491

492 **References**

493

494 Aalto R, Nittrouer CA (2012) 210Pb geochronology of flood events in large tropical river systems.
 495 Philo Trans A Math Phys Eng Sci 370:2040-2074. doi:10.1098/rsta.2011.0607

496 Alric R (2009) Recueil des débits caractéristiques de la Nouvelle Calédonie. In: Direction des Affaires
 497 Vétérinaires Alimentaires et Rurales (DAVAR), Service de l'eau des statistiques et études
 498 rurales. Observatoire de la ressource en eau Nouméa,

499 Batista PVG, Laceby JP, Silva MLN, Tassinari D, Bispo DFA, Curi N, Davies J, Quinton JN (2018) Using
 500 pedological knowledge to improve sediment source apportionment in tropical environments.
 501 J Soils Sediments doi:10.1007/s11368-018-2199-5

502 Bird ECF, Dubois JP, Iltis JA (1984) The impacts of opencast mining on the rivers and coasts of New
 503 Caledonia. Tokyo, Japan, United Nations University.

504 Blake WH, Wallbrink PJ, Wilkinson SN, Humphreys GS, Doerr SH, Shakesby RA, Tomkins KM (2009)
 505 Deriving hillslope sediment budgets in wildfire-affected forests using fallout radionuclide
 506 tracers. Geomorphology 104:105-116. doi:10.1016/j.geomorph.2008.08.004

507 Bottrill L, Walling D, Leeks G (1999) Geochemical characteristics of overbank deposits and their
 508 potential for determining suspended sediment provenance; an example from the River
 509 Severn, UK. Geological Society, London, Special Publications 163:241-257.

510 Brown A, Carpenter R, Walling D (2008) Monitoring the fluvial palynomorph load in a lowland
 511 temperate catchment and its relationship to suspended sediment and discharge.
 512 Hydrobiologia 607:27-40.

513 Collins AL, Walling DE, Leeks GJL (1996) Composite fingerprinting of the spatial source of fluvial
 514 suspended sediment : a case study of the Exe and Severn river basins, United Kingdom.
 515 Géomorphologie : relief, processus, environnement 2:41-53. doi:10.3406/morfo.1996.877

516 Danloux J, Laganier R (1991) Classification et quantification des phénomènes d'érosion, de transport
 517 et de sédimentation sur les bassins touchés par l'exploitation minière en Nouvelle Calédonie.

518 David G, Leopold M, Dumas PS, Ferraris J, Herrenschildt JB, Fontenelle G (2010) Integrated coastal
 519 zone management perspectives to ensure the sustainability of coral reefs in New Caledonia.
 520 Mar Pollut Bull 61:323-334. doi:10.1016/j.marpolbul.2010.06.020

521 Davis CM, Fox JF (2009) Sediment fingerprinting: review of the method and future improvements for
 522 allocating nonpoint source pollution. J Environ Eng 135:490-504.

523 Dumas P, Printemps J, Mangeas M, Luneau G (2010) Developing erosion models for integrated
 524 coastal zone management: a case study of The New Caledonia west coast. Mar Pollut Bull
 525 61:519-529. doi:10.1016/j.marpolbul.2010.06.013

526 Evrard O, Laceby JP, Ficetola GF, Gielly L, Huon S, Lefèvre I, Onda Y, Poulenard J (2019) Environmental
 527 DNA provides information on sediment sources: A study in catchments affected by
 528 Fukushima radioactive fallout. Sci Total Environ 665:873-881.

529 Evrard O, Laceby JP, Huon S, Lefèvre I, Sengtaheuanghoung O, Ribolzi O (2015) Combining multiple
 530 fallout radionuclides (¹³⁷Cs, ⁷Be, ²¹⁰Pbxs) to investigate temporal sediment source
 531 dynamics in tropical, ephemeral riverine systems. J Soils Sediments 16:1130-1144.
 532 doi:10.1007/s11368-015-1316-y

533 Ficetola GF, Poulenard J, Sabatier P, Messenger E, Gielly L, Leloup A, Etienne D, Bakke J, Malet E,
 534 Fanget B (2018) DNA from lake sediments reveals long-term ecosystem changes after a
 535 biological invasion. Sci Adv 4:eaar4292.

536 Foucher A, Laceby PJ, Salvador-Blanes S, Evrard O, Le Gall M, Lefèvre I, Cerdan O, Rajkumar V,
 537 Desmet M (2015) Quantifying the dominant sources of sediment in a drained lowland
 538 agricultural catchment: The application of a thorium-based particle size correction in
 539 sediment fingerprinting. Geomorphology 250:271-281. doi:10.1016/j.geomorph.2015.09.007

540 Garcin M (2010) Exploitation des granulats en lit vif des cours d'eau de la Grande-Terre, Nouvelle-
 541 Calédonie. BRGM/RP-58531-FR. 114 p., 90 fig., 3 tabl. Bureau des Recherches Géologiques et
 542 Minières

543 Garcin M, Gastaldi Y, Lesimple S (2017) Quantification et évolution temporelle des apports miniers
 544 dans les rivières calédoniennes. BRGM/RP-66840-FR, 44 p., 23 fig., 5. Bureau des Recherches
 545 Géologiques et Minières

546
547 Haddadchi A, Ryder DS, Evrard O, Olley J (2013) Sediment fingerprinting in fluvial systems: review of
548 tracers, sediment sources and mixing models. *Int J Sediment Res* 28:560-578.
549 Hancock GJ, Wilkinson SN, Hawdon AA, Keen RJ (2014) Use of fallout tracers ⁷Be, ²¹⁰Pb and ¹³⁷Cs to
550 distinguish the form of sub-surface soil erosion delivering sediment to rivers in large
551 catchments. *Hydrol Process* 28:3855-3874.
552 Hedouin L, Bustamante P, Fichez R, Warnau M (2008) The tropical brown alga *Lobophora variegata* as
553 a bioindicator of mining contamination in the New Caledonia lagoon: a field transplantation
554 study. *Mar Environ Res* 66:438-444. doi:10.1016/j.marenvres.2008.07.005
555 Hedouin L, Pringault O, Metian M, Bustamante P, Warnau M (2007) Nickel bioaccumulation in
556 bivalves from the New Caledonia lagoon: Seawater and food exposure. *Chemosphere*
557 66:1449-1457.
558 Heintz T, Haapkyla J, Gilbert A (2015) Coral health on reefs near mining sites in New Caledonia. *Dis*
559 *Aquat Organ* 115:165-173. doi:10.3354/dao02884
560 IEOM (2016) Rapport d'activité 2016 de la Nouvelle-Calédonie. Institut d'Emission Outre-Mer
561 Koiter A, Owens P, Petticrew E, Lobb D (2013) The behavioural characteristics of sediment properties
562 and their implications for sediment fingerprinting as an approach for identifying sediment
563 sources in river basins. *Earth-Sci Rev* 125:24-42.
564 Krause A, Franks S, Kalma J, Loughran R, Rowan J (2003) Multi-parameter fingerprinting of sediment
565 deposition in a small gullied catchment in SE Australia. *Catena* 53:327-348.
566 Lacey JP, Evrard O, Smith HG, Blake WH, Olley JM, Minella JPG, Owens PN (2017) The challenges
567 and opportunities of addressing particle size effects in sediment source fingerprinting: A
568 review. *Earth-Sci Rev* 169:85-103. doi:10.1016/j.earscirev.2017.04.009
569 Lacey JP, Gellis AC, Koiter AJ, Blake WH, Evrard O (2019) Preface evaluating the response of critical
570 zone processes to human impacts with sediment source fingerprinting. *J Soils Sediments*
571 doi:10.1007/s11368-019-02409-0
572 Lacey JP, McMahon J, Evrard O, Olley J (2015) A comparison of geological and statistical approaches
573 to element selection for sediment fingerprinting. *J Soils Sediments* 15:2117-2131.
574 doi:10.1007/s11368-015-1111-9
575 Lacey JP, Olley J (2015) An examination of geochemical modelling approaches to tracing sediment
576 sources incorporating distribution mixing and elemental correlations. *Hydrol Process*
577 29:1669-1685. doi:10.1002/hyp.10287
578 Le Gall M, Evrard O, Foucher A, Lacey JP, Salvador-Blanes S, Maniere L, Lefevre I, Cerdan O, Ayrault
579 S (2017) Investigating the temporal dynamics of suspended sediment during flood events
580 with ⁷Be and ²¹⁰Pb_{xs} measurements in a drained lowland catchment. *Sci Rep* 7:42099.
581 doi:10.1038/srep42099
582 Le Gall M, Evrard O, Foucher A, Lacey JP, Salvador-Blanes S, Thil F, Dapoigny A, Lefevre I, Cerdan O,
583 Ayrault S (2016) Quantifying sediment sources in a lowland agricultural catchment pond
584 using (¹³⁷Cs activities and radiogenic (⁸⁷Sr)/(⁸⁶Sr ratios. *Sci Total Environ* 566-567:968-
585 980. doi:10.1016/j.scitotenv.2016.05.093
586 Legout C, Poulenard J, Nemery J, Navratil O, Grangeon T, Evrard O, Esteves M (2013) Quantifying
587 suspended sediment sources during runoff events in headwater catchments using
588 spectrophotometry. *J Soils Sediments* 13:1478-1492. doi:10.1007/s11368-013-0728-9
589 Martínez-Carreras N, Udelhoven T, Krein A, Gallart F, Iffly JF, Ziebel J, Hoffmann L, Pfister L, Walling
590 DE (2010) The use of sediment colour measured by diffuse reflectance spectrometry to
591 determine sediment sources: application to the Attert River catchment (Luxembourg). *J*
592 *Hydrol* 382:49-63.
593 Mertes LA (1994) Rates of flood-plain sedimentation on the central Amazon River. *Geology* 22:171-
594 174.
595 Nyman P, Sheridan GJ, Smith HG, Lane PNJ (2011) Evidence of debris flow occurrence after wildfire in
596 upland catchments of south-east Australia. *Geomorphology* 125:383-401.
597 doi:10.1016/j.geomorph.2010.10.016

598 Olley J, Brooks A, Spencer J, Pietsch T, Borombovits D (2013) Subsoil erosion dominates the supply of
599 fine sediment to rivers draining into Princess Charlotte Bay, Australia. *J Environ Radioact*
600 124:121-129. doi:10.1016/j.jenvrad.2013.04.010

601 Olley J, Caitcheon G (2000) Major element chemistry of sediments from the Darling–Barwon river
602 and its tributaries: implications for sediment and phosphorus sources. *Hydrol Process*
603 14:1159-1175.

604 Owens PN, Walling DE (2002) The phosphorus content of fluvial sediment in rural and industrialized
605 river basins. *Water Res* 36:685-701.

606 Owens PN, Walling DE, Carton J, Meharg AA, Wright J, Leeks GJL (2001) Downstream changes in the
607 transport and storage of sediment-associated contaminants (P, Cr and PCBs) in agricultural
608 and industrialized drainage basins. *Sci Total Environ* 266:177-186.

609 Pascal M, De Forges BR, Le Guyader H, Simberloff D (2008) Mining and other threats to the New
610 Caledonia biodiversity hotspot. *Conserv Biol* 22:498-499.

611 Pascal N (2010) Ecosystèmes coralliens de Nouvelle-Calédonie Valeur économique des services
612 écosystémiques Partie I: Valeur financière. IFRECOR Nouvelle-Calédonie, Nouméa 155

613 Restrepo JD, Park E, Aquino S, Latrubesse EM (2016) Coral reefs chronically exposed to river
614 sediment plumes in the southwestern Caribbean: Rosario Islands, Colombia. *Sci Total Environ*
615 553:316-329. doi:10.1016/j.scitotenv.2016.02.140

616 Rogers CS (1979) The effect of shading on coral reef structure and function. *J Exp Mar Biol Ecol*
617 41:269-288.

618 Rogers CS (1990) Responses of coral reefs and reef organisms to sedimentation. *Mar Ecol Prog Ser*
619 62:185-202.

620 Sabinot C, Lacombe S (2015) La pêche en tribu face à l'industrie minière dans le sud-est de la
621 Nouvelle-Calédonie. In: *Rev. Société Int. D'Ethnographie* 5, La mer et les Hommes. pp 120-
622 137

623 Schwertmann U, Latham M (1986) Properties of iron oxides in some New Caledonian oxisols.
624 *Geoderma* 39:105-123.

625 Sevin B (2014) Cartographie du régolithe sur formation ultrabasique de Nouvelle-Calédonie:
626 Localisation dans l'espace et le temps des gisements nickélicifères. Nouvelle Calédonie

627 Shellberg J, Brooks A, Spencer J Land-use change from indigenous management to cattle grazing
628 initiates the gullyng of alluvial soils in northern Australia. In: *19th World Congress of Soil*
629 *Science: Soil Solutions for a Changing World, 2010*. pp 1-6

630 Sherriff SC, Franks SW, Rowan JS, Fenton O, Ó'hUallacháin D (2015) Uncertainty-based assessment of
631 tracer selection, tracer non-conservativeness and multiple solutions in sediment
632 fingerprinting using synthetic and field data. *J Soils Sediments* 15:2101-2116.
633 doi:10.1007/s11368-015-1123-5

634 Smith HG, Sheridan GJ, Lane PNJ, Noske PJ, Heijnis H (2011) Changes to sediment sources following
635 wildfire in a forested upland catchment, southeastern Australia. *Hydrol Process* 25:2878-
636 2889. doi:10.1002/hyp.8050

637 Smith HG, Sheridan GJ, Nyman P, Child DP, Lane PNJ, Hotchkis MAC, Jacobsen GE (2012) Quantifying
638 sources of fine sediment supplied to post-fire debris flows using fallout radionuclide tracers.
639 *Geomorphology* 139-140:403-415. doi:10.1016/j.geomorph.2011.11.005

640 Stout JC, Belmont P, Schottler SP, Willenbring JK (2013) Identifying Sediment Sources and Sinks in the
641 Root River, Southeastern Minnesota. *Ann Assoc Am Geogr* 104:20-39.
642 doi:10.1080/00045608.2013.843434

643 Terry JP, Garimella S, Kostaschuk RA (2002) Rates of floodplain accretion in a tropical island river
644 system impacted by cyclones and large floods. *Geomorphology* 42:171– 182.

645 Terry JP, Kostaschuk RA, Wotling G (2008) Features of tropical cyclone-induced flood peaks on
646 Grande Terre, New Caledonia. *Water Environ J* 22:177-183. doi:10.1111/j.1747-
647 6593.2007.00098.x

648 Trescases JJ (1973) Weathering and geochemical behaviour of the elements of ultramafic rocks in
649 New Caledonia. *BMRJ Aust Geol and Geophys* 141:149-161.

650 Wallbrink P, Murray A, Olley J, Olive L (1998) Determining sources and transit times of suspended
651 sediment in the Murrumbidgee River, New South Wales, Australia, using fallout ¹³⁷Cs and
652 ²¹⁰Pb. *Water Resour Res* 34:879-887.

653 Walling D, Peart M, Oldfield F, Thompson R (1979) Suspended sediment sources identified by
654 magnetic measurements. *Nature* 281:110.

655 Walling DE (2005) Tracing suspended sediment sources in catchments and river systems. *Sci Total*
656 *Environ* 344:159-184. doi:10.1016/j.scitotenv.2005.02.011

657 Walling DE (2013) The evolution of sediment source fingerprinting investigations in fluvial systems. *J*
658 *Soils Sediments* 13:1658-1675. doi:10.1007/s11368-013-0767-2

659 Walling DE, Owens PN, Carter J, Leeks GJL, Lewis S, Meharg AA, Wright J (2003) Storage of sediment-
660 associated nutrients and contaminants in river channel and floodplain systems. *Applied*
661 *Geochemistry* 18:195-220.

662 Wilkinson SN, Hancock GJ, Bartley R, Hawdon AA, Keen RJ (2013) Using sediment tracing to assess
663 processes and spatial patterns of erosion in grazed rangelands, Burdekin River basin,
664 Australia. *Agric Ecosyst Environ* 180:90-102. doi:10.1016/j.agee.2012.02.002

665

666

667 **Tables**

668 **Table 1** Fallout radionuclide activities and geogenic radionuclide contents (mean, M; standard deviation, SD) in
669 the <2 mm and <63 µm fractions of sediment sources and Thio river sediment.

670 **Table 2** Results of Mann-Whitney U test and the DFA used to identify the optimum tracer combination to
671 differentiate sources supplying sediment to the Thio River for the <2 mm particle size fraction with the geogenic
672 approach and for the <63 µm particle size fraction with the geochemical approach.

673 **Table 3** Source contributions calculated by both approaches using gamma spectrometry or X-Ray Fluorescence
674 measurements for sediment deposited during the flood of February 25, 2015.

675 **Table 4** Source contributions calculated by both approaches using gamma spectrometry or X-Ray Fluorescence
676 measurements for sediment deposited during the flood of April 10, 2017.

677

678

679

Table 1

		Mining tributaries (<i>n</i> =16)				Non-mining tributaries (<i>n</i> =8)				Thio river sediment 2015 (<i>n</i> =11)				Thio river sediment 2017 (<i>n</i> =8)			
Fingerprinting property	Particle size	M	SD	Min	Max	M	SD	Min	Max	M	SD	Min	Max	M	SD	Min	Max
¹³⁷ Cs (<i>Bq kg⁻¹</i>)	<2 mm	0.3	0.1	0.1	0.6	0.6	0.3	0.3	1.2	0.7	0.1	0.2	1.3	0.5	0.4	0.1	0.5
	<63 μm	0.3	0.3	0.01	0.9	1	0.5	0.5	1.4	0.7	0.4	0.2	1.3	ND	ND	ND	ND
²¹⁰ Pb _{xs} (<i>Bq kg⁻¹</i>)	<2 mm	3	3	1	12	10	10	2	34	9	5	4	18	8	5	2	15
	<63 μm	6	7	0.1	19	19	15	7	44	15	8	6	44	ND	ND	ND	ND
K (<i>mg kg⁻¹</i>)	<2 mm	1386	1848	57	5973	12097	3980	5181	17296	4711	2270	1593	9347	2792	880	1691	4292
	<63 μm	1140	1298	121	4742	12051	1394	10060	13697	5969	3030	1979	9240	ND	ND	ND	ND
Th (<i>mg kg⁻¹</i>)	<2 mm	0.6	0.7	0.08	2	6	2	2	7	1	0.6	0.6	6	2	1	0.6	2
	<63 μm	0.5	0.4	0.1	1	7	1	6	8	3	2	0.8	6	ND	ND	ND	ND
U (<i>mg kg⁻¹</i>)	<2 mm	0.1	0.1	0.04	0.5	1.2	0.3	0.3	1.5	0.3	0.1	0.2	1.2	0.4	0.3	0.4	0.4
	<63 μm	0.1	0.1	0.05	0.2	1.3	0.1	1.2	1.5	0.6	0.3	0.2	1	ND	ND	ND	ND

Table 2

Fingerprinting property	Mann-Whitney U test		DFA- backward mode			
	U value	p value	Wilk's Lambda	Variance explained by the variables (%)	Squared Mahalanobis distance	Correctly classified samples (%)
^{137}Cs (Bq kg^{-1})	38	0.7720	-	-	-	-
$^{210}\text{Pb}_{\text{xs}}$ (Bq kg^{-1})	16	0.1109	-	-	-	-
K (mg kg^{-1})	2	< 0.0001	-	-	-	-
Th (mg kg^{-1})	2	< 0.0001	-	-	-	-
U (mg kg^{-1})	2	< 0.0001	0.1742	82.6	19.6	96
Al (mg kg^{-1})	8	0.000	-	-	-	-
Ca (mg kg^{-1})	21	0.007	-	-	-	-
Cr (mg kg^{-1})	124	< 0.0001	-	-	-	-
Cu (mg kg^{-1})	23	0.011	-	-	-	-
Fe (mg kg^{-1})	121	0.000	-	-	-	-
K (mg kg^{-1})	2	< 0.0001	0.1691	83.1	20.3	96
Mg (mg kg^{-1})	119	0.000	-	-	-	-
Mn (mg kg^{-1})	108	0.006	-	-	-	-
Ni (mg kg^{-1})	125	< 0.0001	-	-	-	-
Si (g kg^{-1})	6	< 0.0001	-	-	-	-
Ti (mg kg^{-1})	13	0.001	-	-	-	-
Zn (mg kg^{-1})	68	0.834	-	-	-	-

Table 3

Sampling point	Mining tributary contribution (%)		Non mining tributary contributions (%)	
	U – Gamma spectrometry	K – XRF	U – Gamma spectrometry	K – XRF
1	97	95	3	5
2	96	95	4	5
3	5	20	95	80
4	64	69	36	31
5	75	46	25	54
6	76	79	24	21
7	11	33	89	67
8	79	86	21	14
9	86	89	14	11
10	80	69	20	31
11	82	63	18	37
M (%)	68	68	32	32
SD (%)	31	25	31	25
Minimum (%)	5	46	3	5
Maximum (%)	97	95	95	80

Table 4

Sampling point	Mining tributary contribution (%)		Non mining tributary contributions (%)	
	U – Gamma spectrometry	K – XRF	U – Gamma spectrometry	K – XRF
1	96	90	4	10
2	96	93	4	7
3	95	90	5	10
4	76	73	24	27
5	84	83	16	17
6	79	81	21	19
7	86	79	14	21
8	86	84	14	16
M (%)	87	84	13	16
SD (%)	8	7	8	7
Minimum (%)	76	73	4	7
Maximum (%)	96	93	24	27

680 **Figure captions**

681 **Fig. 1** Main lithologies (a.), the location of rainfall and river monitoring stations (b.) and the sediment samples
682 collected along with tributary source classifications and the location of the active and abandoned mining sites
683 along with mining exploration (c.) conducted in the Thio catchment, New Caledonia

684 **Fig. 2** Box-plots of fallout radionuclide activities (i.e. ^{137}Cs , $^{210}\text{Pb}_{\text{xs}}$) in the <2 mm (a) and the <63 μm (b)
685 fractions of sediment collected on the mining tributaries (Mining), non-mining tributaries (Non mining) and the
686 main Thio River (Thio river sediment (TRS) - flood events of 2015 and 2017). The box indicates the location of
687 the first and third quartiles; the black line indicates the median value; the red line indicates the mean value

688 **Fig. 3** Comparison of ^{137}Cs (a) and $^{210}\text{Pb}_{\text{xs}}$ (b) activities measured in the <63 μm and the <2 mm fractions of
689 sediment samples collected in the Thio River catchment

690 **Fig. 4** Box-plots of geogenic radionuclide contents (i.e. K, Th, U) in the <2 mm fraction of sediment collected on
691 the mining tributaries (Mining), non-mining tributaries (Non mining) and the main Thio River (Thio river
692 sediment (TRS) - flood events of 2015 and 2017). The box indicates the location of the first and third quartiles;
693 the black line

694 **Fig. 5** Comparison of K (a), Th (b) and U (c) contents measured in the <63 μm and the <2 mm fractions of
695 sediment samples collected in the Thio River catchment

696 **Fig. 6** Box-plots of geochemical element contents in the $<63\mu\text{m}$ fraction of sediment collected on the mining
697 tributaries (Mining), non-mining tributaries (Non-mining) and the main Thio River (Thio river sediment (TRS) -
698 flood events of 2015 and 2017). The box indicates the location of the first and third quartiles; the black line
699 indicates the median value; the red line indicates the mean value

700 **Fig. 7** Comparison of geochemical elemental contents measured in the <63 μm and the <2 mm fractions of sediment
701 samples collected in the Thio River catchment

702 **Fig. 8** Relative contributions of mining and non-mining tributaries to the sediment collected in the Thio River
703 (2015 Flood Event) on the <2 mm fraction measurements using the geogenic model (U)

704 **Fig. 9** Relative contributions of mining and non-mining tributaries to the sediment collected in the Thio River
705 (2017 Flood event) based on the <2 mm fraction measurements using the geogenic model (U)

706

707

Fig. 1

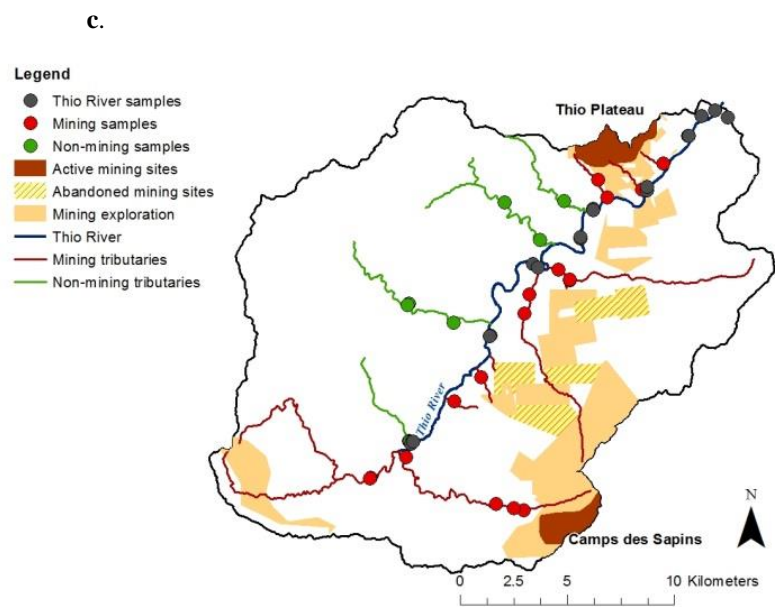
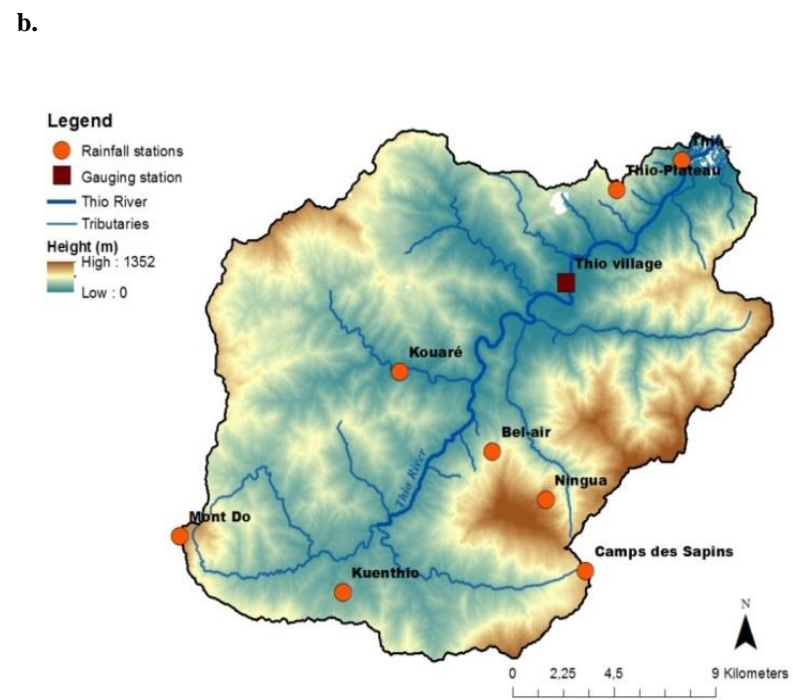
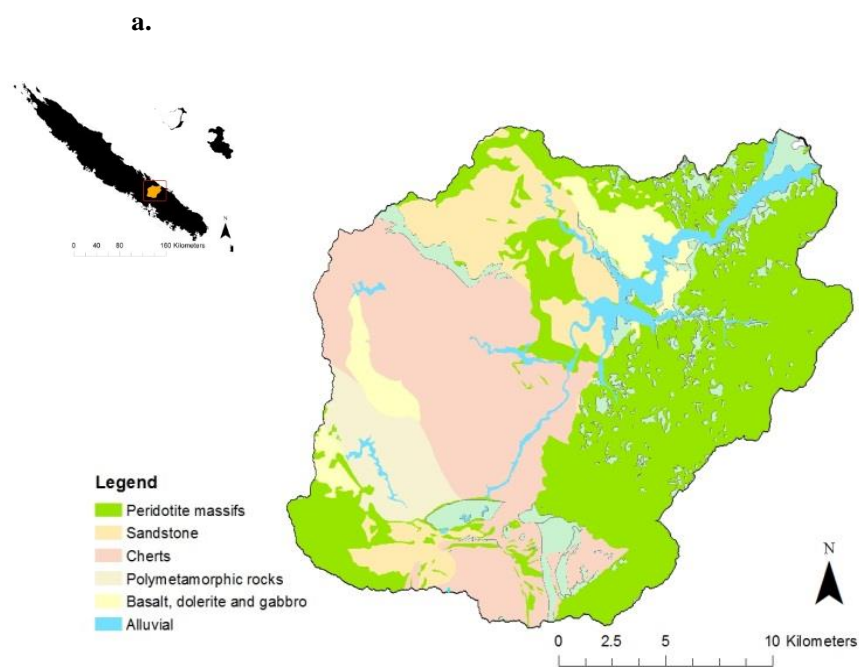
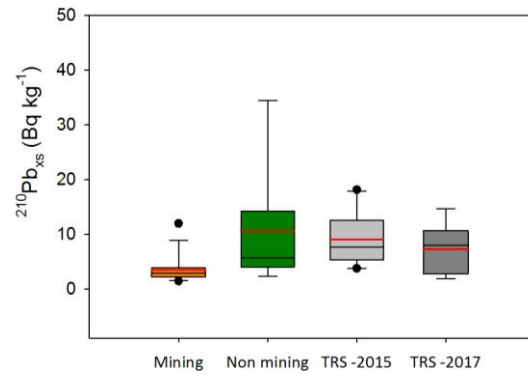
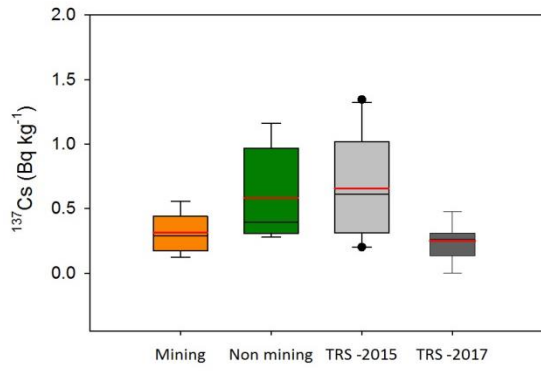


Fig. 2

a. <2 mm



b. <63 μm

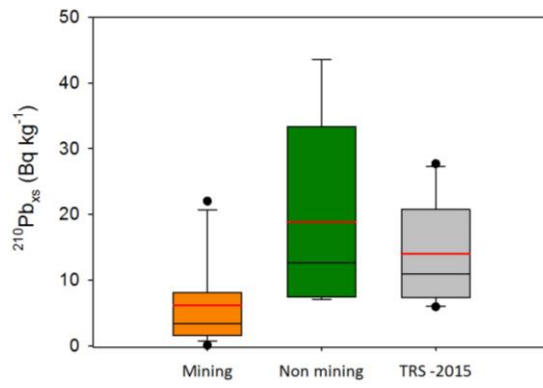
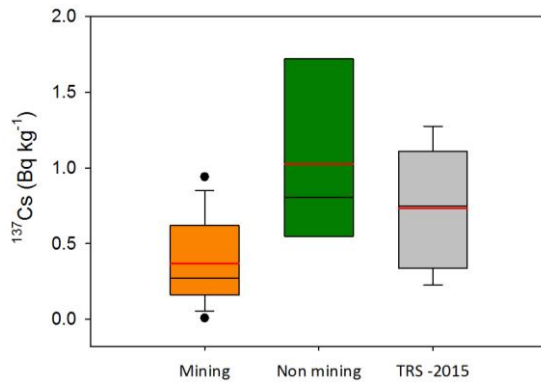
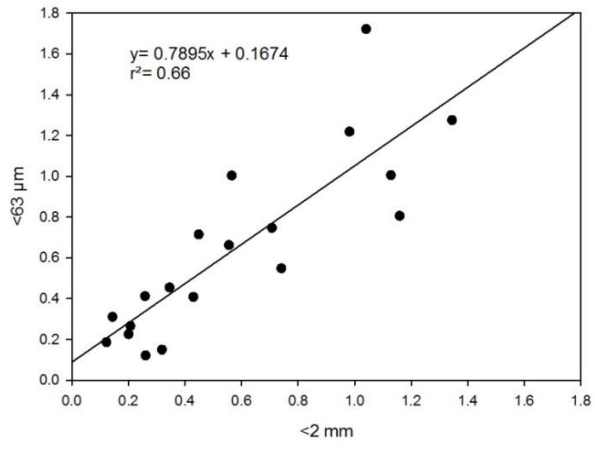


Fig. 3

a. ^{137}Cs (Bq kg^{-1})



b. $^{210}\text{Pb}_{\text{xs}}$ (Bq kg^{-1})

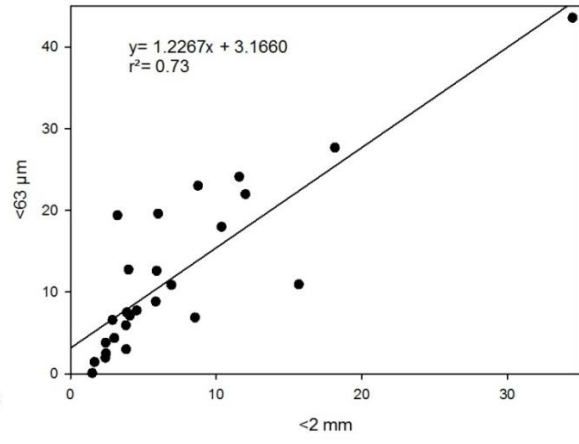


Fig. 4

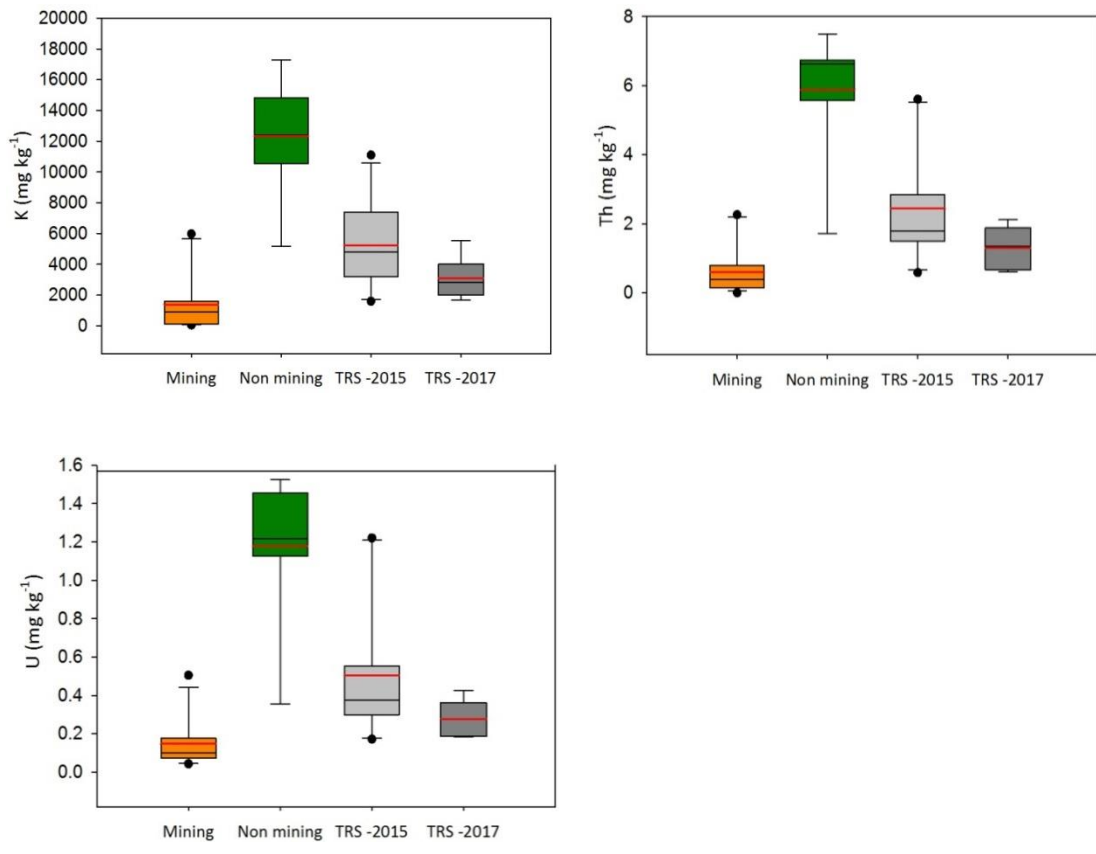


Fig.5

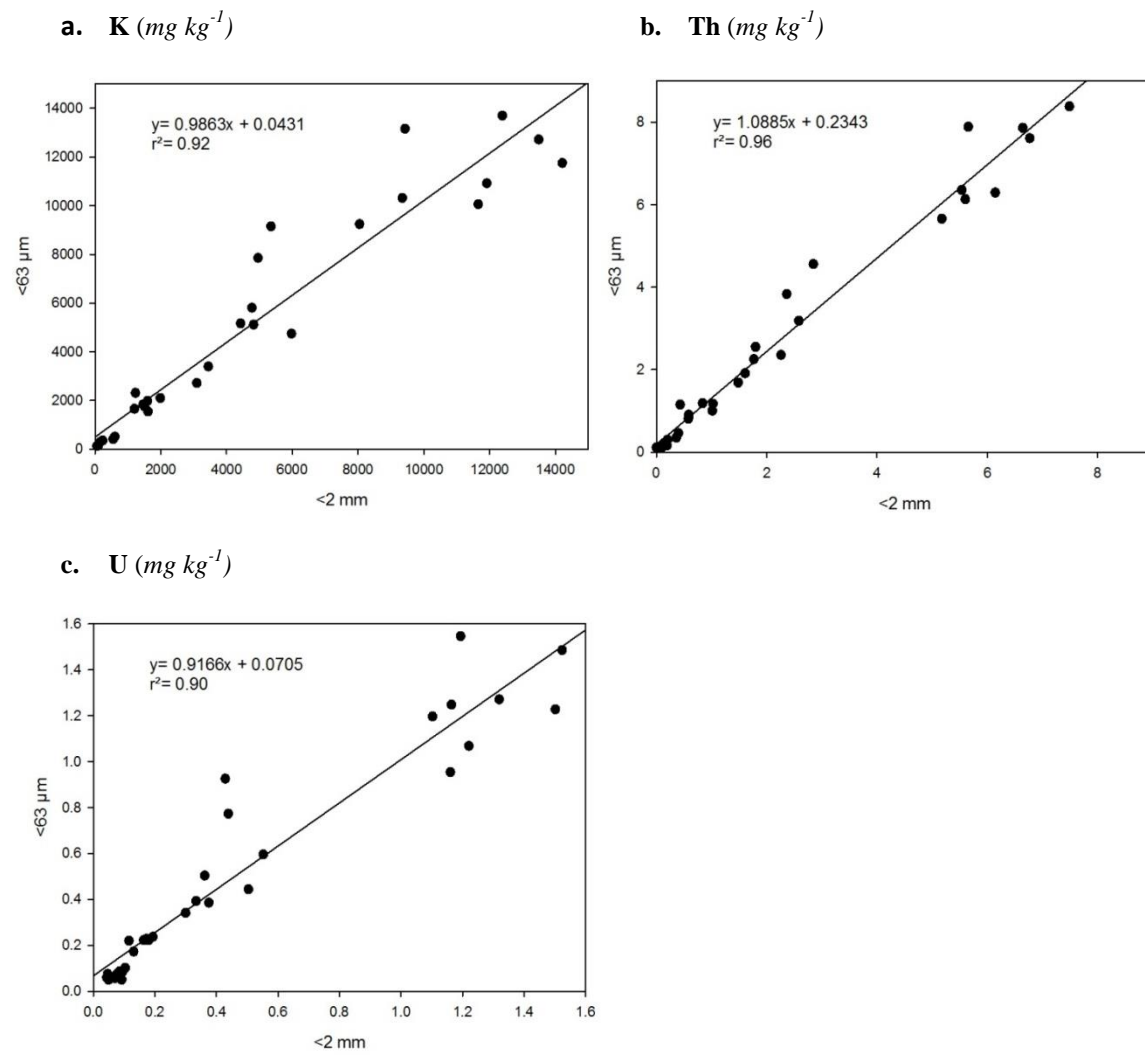


Fig. 6

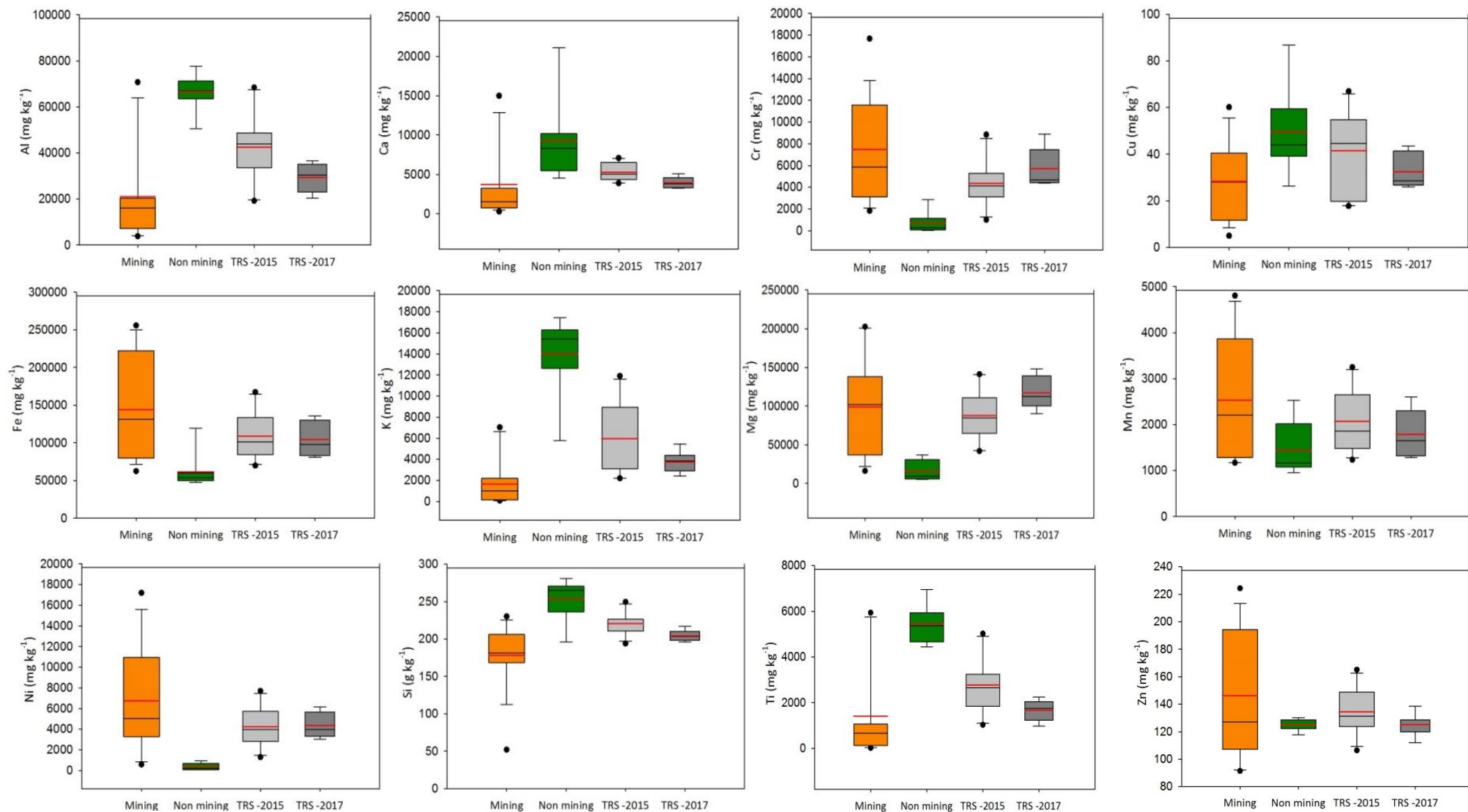


Fig. 7

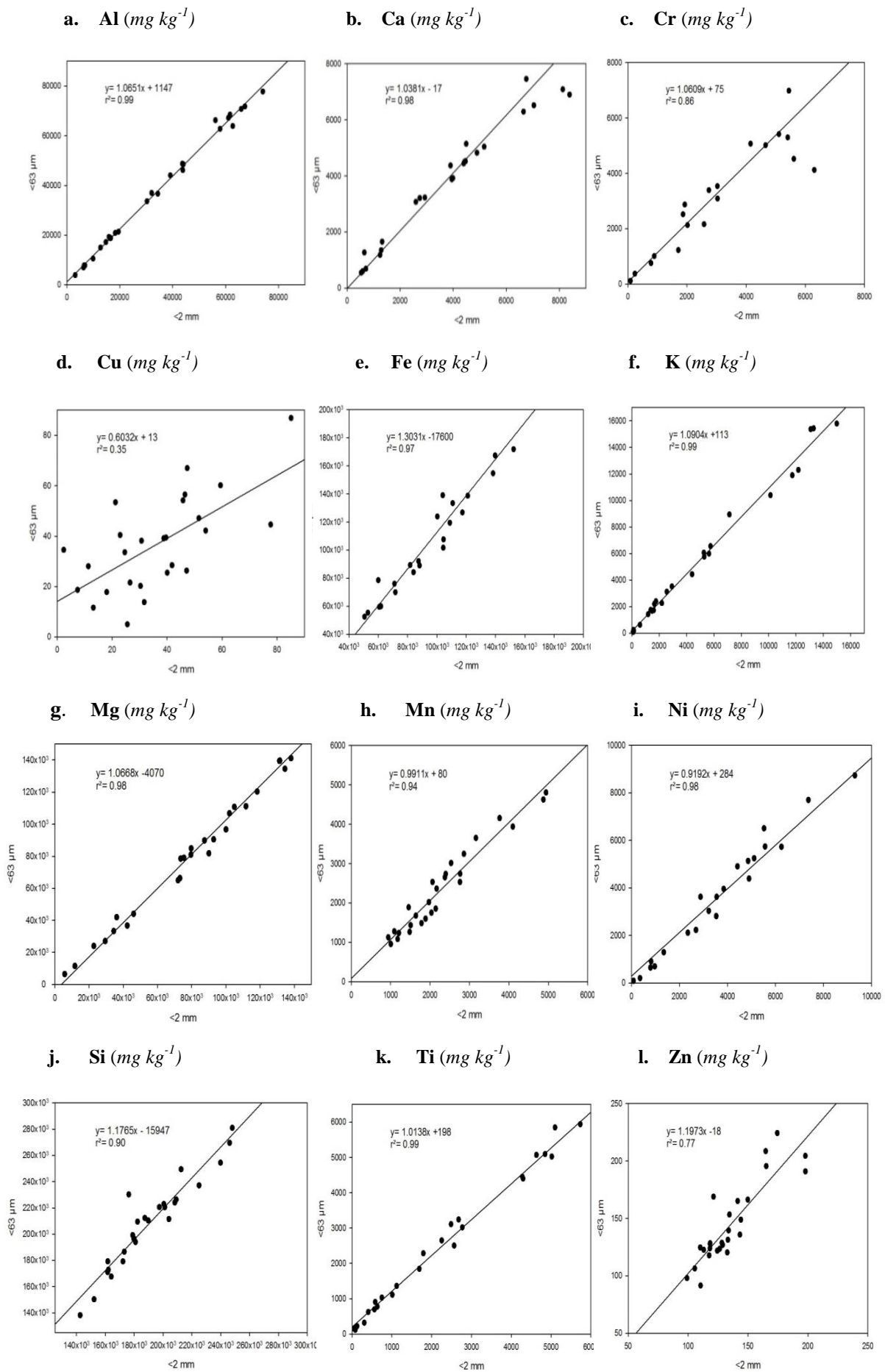

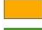






Fig. 8

2015 flood event

Legend

Source contributions (%)

-  Source contributions (%)
-  Mining tributaries
-  Non-mining tributaries
-  Active mining sites
-  Abandoned mining sites
-  Mining exploration
-  Thio River
-  Mining tributaries
-  No-mining tributaries

- a. Watou
- b. Fanama
- c. Kouaré
- d. Kouergoa
- e. Koua
- f. Creek des Japonais
- g. Creek Jeanne et Marie
- h. Nakalé
- i. Nembrou
- j. Creek cimetièrre
- k. Mué
- l. Tomuru

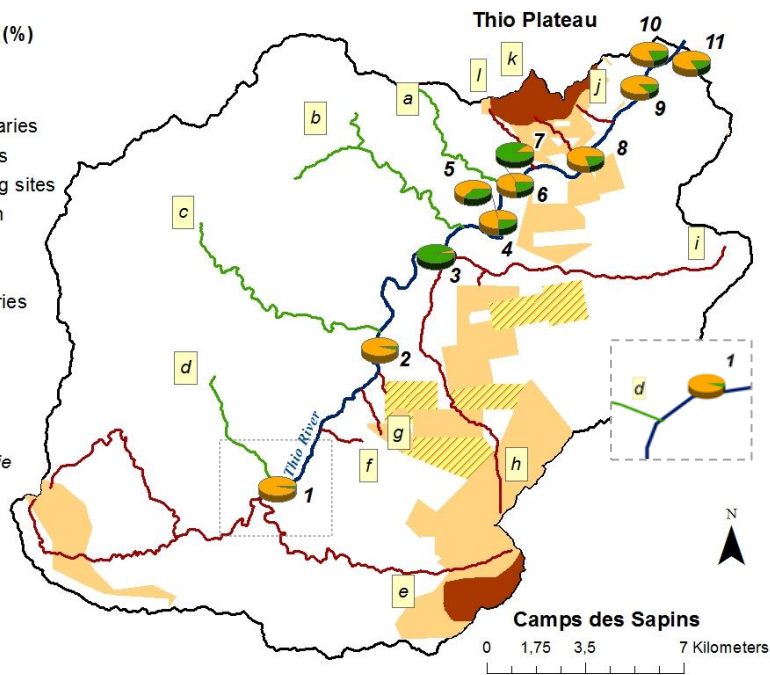
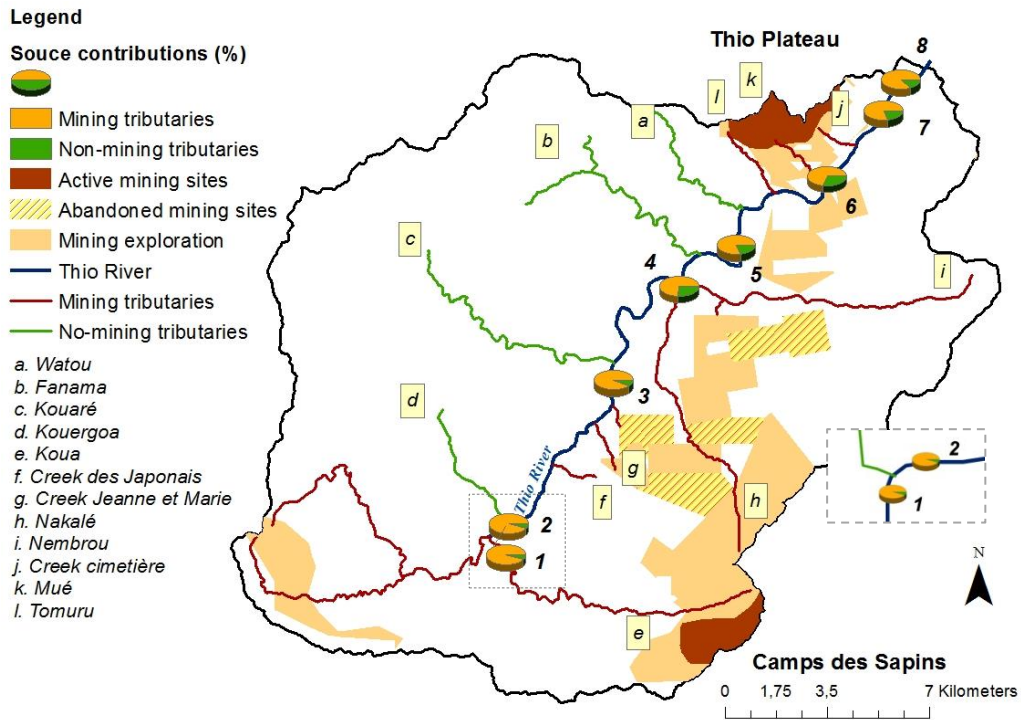


Fig. 9

2017 flood event



708 **Supplementary Material**

709 Fig. A1 Spatial rainfall distribution during flood events of February 25, 2015 (a) and April 10, 2017 (b) on the

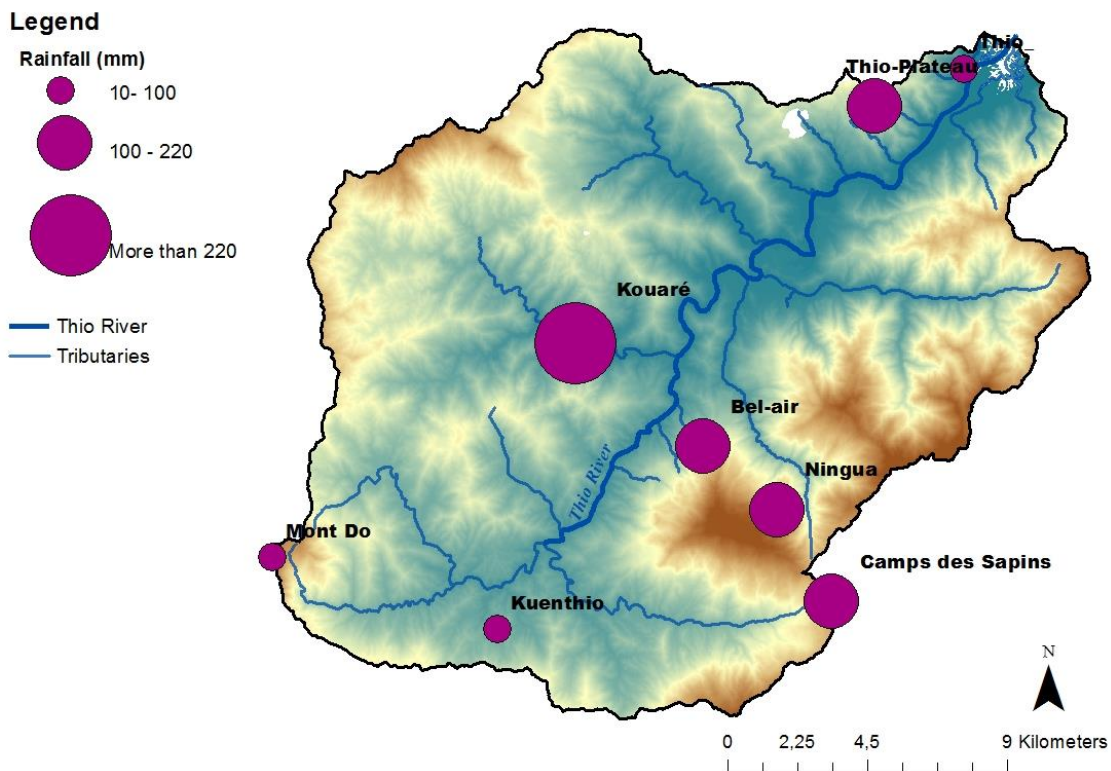
710 Thio River catchment

711

Supplementary Material

Fig. A1

a.



b.

